CrossMark

OGLE-ing the Magellanic System: RR Lyrae Stars in the Bridge[*]

Anna M. Jacyszyn-Dobrzeniecka[1,2] , Przemek Mróz[1,5] , Katarzyna Kruszyńska[1], Igor Soszyński[1] , Dorota M. Skowron[1],
Andrzej Udalski[1], Michał K. Szymański[1], Patryk Iwanek[1] , Jan Skowron[1] , Paweł Pietrukowicz[1] , Radosław Poleski[3] ,
Szymon Kozłowski[1] , Krzysztof Ulaczyk[4] , Krzysztof Rybicki[1], and Marcin Wrona[1]

[1] Astronomical Observatory, University of Warsaw, Al. Ujazdowskie 4, 00-478 Warszawa, Poland; jacyszyn@uni-heidelberg.de
[2] Astronomisches Rechen-Institut, Zentrum für Astronomie der Universität Heidelberg, Mönchhofstr. 12-14, D-69120 Heidelberg, Germany
[3] Department of Astronomy, Ohio State University, 140 West 18th Avenue, Columbus, OH 43210, USA
[4] Department of Physics, University of Warwick, Coventry CV4 7AL, UK
[5] Division of Physics, Mathematics, and Astronomy, California Institute of Technology, Pasadena, CA 91125, USA

Abstract

We use the extended and updated Optical Gravitational Lensing Experiment (OGLE) Collection of Variable Stars
to thoroughly analyze the distribution of RR Lyrae stars in the Magellanic Bridge. We use photometric metallicities
to derive the absolute Wesenheit magnitude and individual distance of each RR Lyrae star. We confirm results
from our earlier study showing that RR Lyrae stars are present in between the Magellanic Clouds, though their
three-dimensional distribution more resembles two extended overlapping structures than a strict bridge-like
connection. The contours do connect in the southern parts of the Bridge, albeit on a level too low to state that an
evident connection exists. To test the sample numerically, we use multi-Gaussian fitting and conclude that there is
no additional population or overdensity located in the Bridge. We also try to reproduce results on the putative RR
Lyrae Magellanic Bridge stream by selecting RR Lyrae candidates from *Gaia* Data Release 1. We show that we are
not able to obtain the evident connection of the Clouds without many spurious sources in the sample, as the cuts are
not able to remove artifacts without eliminating the evident connection at the same time. Moreover, for the first
time, we present the *Gaia* Data Release 2 RR Lyrae stars in the Magellanic Bridge area and show that their
distribution matches our results.

Key words: galaxies: Magellanic Clouds – stars: variables: RR Lyrae

1. Introduction

Interactions between the Magellanic Clouds, and probably
between the pair and the Milky Way, led to the formation of an
entire complex of structures, together with the Clouds, referred to
as the Magellanic System (e.g., Gardiner et al. 1994; Gardiner &
Noguchi 1996; Yoshizawa & Noguchi 2003; Connors et al. 2006;
Růžička et al. 2009, 2010; Besla et al. 2010, 2012; Diaz & Bekki
2012a, 2012b; Guglielmo et al. 2014). One piece of evidence of
the latest encounter of the Large and Small Magellanic Clouds
(LMC and SMC, respectively) is the Magellanic Bridge (MBR;
i.e., Harris 2007).

Many studies proved that there are young stars located in
between the LMC and SMC (Shapley 1940; Irwin et al. 1985;
Demers & Battinelli 1998; Harris 2007; Nöel et al. 2013, 2015),
and moreover, that they form a continuous connection matching
the neutral hydrogen (H I) contours (Skowron et al. 2014). The
young ages of some objects suggest an in situ Bridge formation
(e.g., Jacyszyn-Dobrzeniecka et al. 2016, 2020, hereafter Paper I
and Paper III, respectively). This implies that the interactions
were strong enough to pull out gas from the Magellanic Clouds
and trigger star formation outside these galaxies. For a better
understanding of the processes leading to these events, it is also
important to test the older stellar populations in the MBR. Were
the interactions strong enough to pull out not only gas but also
stars from either the LMC, the SMC, or both? Hereafter, we
focus on the older population of stars. For more information
about different characteristics of the Bridge, see the introduction
in Paper III.

Candidates for a stellar Bridge counterpart belonging to the
older population were found by Bagheri et al. (2013) and
Skowron et al. (2014). Wagner-Kaiser & Sarajedini (2017)
analyzed RR Lyrae (RRL) stars using the Optical Gravitational
Lensing Experiment (OGLE) collection of RRL stars and
demonstrated that there exists a continuous flow of these objects
between the Magellanic Clouds. The authors pointed out that the
metallicities and distances of old population members show a
smooth transition between the LMC and SMC. Moreover, the
RRL star distribution does not match the H I density distribution.
Thus, they suggest that RRL stars better resemble two
overlapping structures than a tidally stripped bridge. Recently,
Zivick et al. (2019) used *Gaia* data to show that an old stellar
population is more broadly distributed and does not follow the
H I bridge, in contrast to a young population.

Jacyszyn-Dobrzeniecka et al. (2017, hereafter Paper II) also
used the RRL sample from the OGLE Collection of Variable
Stars (OCVS; Soszyński et al. 2016) to analyze the three-
dimensional distribution of RRL stars in the Magellanic System
and the Bridge. Their results are perfectly consistent with those
of Wagner-Kaiser & Sarajedini (2017), showing that there is
little evidence for a bridge-like structure formed by an old
population between the Magellanic Clouds.

On the other hand, Carrera et al. (2017) studied 39
intermediate-age and old stars in two Bridge fields located
near the highest H I density contours and close to the SMC
(between R.A. 2ʰ and 3ʰ) and found that, based on chemistry
and kinematics, these objects are tidally stripped from the
SMC. Their metallicities are consistent with those of Wagner-
Kaiser & Sarajedini (2017). Both results are not necessarily
incoherent, as stars analyzed by Carrera et al. (2017) may just

---

be SMC halo members. Their kinematics are in agreement with recent studies by Oey et al. (2018) and Zivick et al. (2019), who found that both young and old stellar populations are moving away from the SMC toward the LMC.

Another study of the Bridge old population was carried out using *Gaia* Data Release 1 (DR1; Gaia Collaboration et al. 2016). Belokurov et al. (2017, hereafter B17) developed a procedure to select RRL candidates from DR1 and analyzed their distribution in the MBR. They found an evident stellar bridge between the Magellanic Clouds that is shifted from the young star bridge, and thus from the highest H I density contours, by about 5°. They explained this difference with an older bridge trailing rather than following the Magellanic System. Moreover, they also performed a simulation to test whether such a scenario is plausible. Later, at least one stellar substructure partially cospatial with the B17 RRL bridge was found by Mackey et al. (2018), who used a deep panoramic survey conducted with the Dark Energy Camera. Also, Belokurov & Erkal (2018) found such substructures in the red giant distribution using *Gaia* Data Release 2 (DR2).

Similarly to B17, Deason et al. (2017) selected Mira candidates from DR1 and analyzed their distribution in the Magellanic System. They found that there are not as many Miras as RRL stars in the Bridge, and no bridge-like connection could be found. However, Miras form a slightly extended feature stretching out of the SMC toward the RRL bridge discovered by B17.

In this paper, which is the fourth in a series devoted to analysis of three-dimensional structure of the Magellanic System using the OCVS, we examine the RRL star distribution in the Bridge area with extended and updated OGLE data. We also compare our results to those of B17, whose results are not in agreement with Paper II. Moreover, we perform an analysis of the DR1 data using the B17 method and show their distribution of RRL candidates. We also show, for the first time, the distribution of RRL stars from *Gaia* DR2 (Gaia Collaboration et al. 2018; Holl et al. 2018; Clementini et al. 2019) in the Bridge area.

We have organized the paper as follows. Section 2 describes the RRL stars from the OCVS and the updates, corrections, and extensions that were later applied to the collection. Sample selection, as well as the methods used for analysis, are found in Section 3. In Section 4 we describe a study of the three-dimensional distribution of RRL stars from the OCVS. Section 5 presents a reanalysis of the OCVS sample using a different method, which is an attempt to reproduce the B17 results. In Section 6 we present our analysis of DR1 data using the B17 method to select RRL candidates. In Section 7 we compare distributions of different stellar tracers in the Bridge and present the DR2 RRL star distribution. We conclude the paper in Section 8.

2. Observational Data

2.1. OCVS

Since Paper II was published, the OCVS has been updated, and a number of new RRL pulsators were added (Soszyński et al. 2016, 2017, 2019). In this paper, similarly to Paper III, we use the newest data from the OCVS. The largest number of newly included objects was added from the newest fields located east and south of the LMC—almost 1000 RRL stars. The newest fields in the southern parts of the MBR resulted in

an addition of over 100 RRL pulsators. For a current OGLE-IV footprint with the newly added fields and the on-sky distribution of all OCVS RRL stars, see Figure 1. For more technical details about the fourth phase of the OGLE project, see Udalski et al. (2015).

3. Data Analysis

3.1. Sample Selection

In our basic approach, we use a very similar method to Paper II. Hereafter, we only analyze the RRab stars, as these are the most common type, and about 70% of all RRL stars pulsate solely in the fundamental mode (i.e., see number of RRL stars published by Soszyński et al. 2011, 2014, 2016, 2017).

We select a few different samples from the entire OGLE collection of RRL stars in the Magellanic System. The first sample (hereafter the entire sample) contains all of the RRab stars and can only be represented in the on-sky maps, as we are not able to calculate distance for each star in this sample. All of the RRab stars for which we were able to calculate distance constitute the second sample (hereafter the uncleaned sample). These stars must have both *I*- and *V*-passband magnitudes and a well-estimated ϕ_{31} coefficient (this is one of the light-curve Fourier decomposition parameters; Simon & Lee 1981). To create the third sample (the cleaned sample), we made an additional cut on the Bailey diagram, the same as we did in Paper II (see Section 2.2 and Figure 1 therein for more details). Then we fit period–luminosity (PL) relations to the second sample using the Wesenheit magnitude and iteratively applied 3σ clipping to the data after each fit (see Section 3.1 in Paper II for more details). The number of RRL stars in each sample is presented in Table 1. Any other additional cuts or selections made to the three described samples are discussed later.

Taking into account the updates made and less complicated cleaning process, this sample should not be identical to our Paper II sample.

3.2. Individual Distances and Coordinates

To calculate individual distances of RRab stars, we use exactly the same method as we did in Paper II and Skowron et al. (2016). We use the Fourier coefficient ϕ_{31}, which we obtained from Fourier decomposition of OGLE light curves, to determine the photometric metallicity (we apply the relation from Nemec et al. 2013). Then we use relations from Braga et al. (2015) to calculate absolute Wesenheit magnitudes. We are aware that their relations are not best suited to our data set, as they were derived for the M4 cluster with different value of R_V. This will cause a systematic shift in our distances and will not influence the geometry of obtained distributions. We continue to use these relations to keep our calculations consistent with Paper II. Having photometric metallicity, as well as absolute and observed magnitudes, we were able to determine the distance to each RRab star. For more details on the relations used and exact transformations, see Section 3.2 in Paper II and Section 5 in Skowron et al. (2016).

Similarly to Jacyszyn-Dobrzeniecka et al. (2016, 2017) and Paper III, we use a Hammer equal-area projection for on-sky plots and the Cartesian three-dimensional coordinate system. The exact equations can be found in Section 3.2 of Paper III (Equations (1)–(5)).
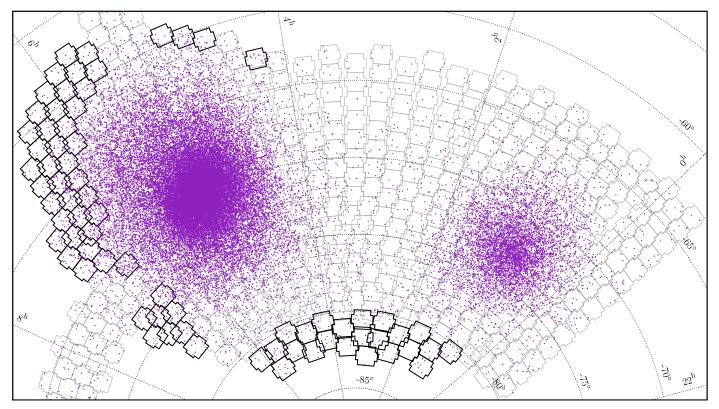
Figure 1. On-sky locations of RRL stars in the Magellanic System. Black contours show the newest additions to the OGLE-IV fields, while gray ones show the main OGLE-IV fields in the Magellanic System that were already observed before 2017 July.

Table 1
Number of RRL Stars in the Samples

Sample	Number
Entire	34,177
Uncleaned	30,675
Cleaned	27,212

4. OGLE RRL Sample

4.1. Three-dimensional Distribution

Figure 2 shows top (upper row) and front (bottom row) view of the three-dimensional distribution of RRab stars in the Magellanic System. The plots were made using two-dimensional Cartesian space projections. The left panels show the uncleaned sample with a clearly visible "blend artifact" in the LMC. This is a nonphysical structure that seems to be emanating from the LMC center and is caused by blending and crowding effects (for a more detailed description, see Section 2.2 and Figure 3 in Paper II). The blend artifact is not protruding and elongated in the next panels, where we show the cleaned sample. The three middle panels show the same sample but with different bin sizes. The contours fitted to the middle panels (medium-sized bins) are shown in the right panels. The lines are on the levels of 1, 5, 20, and 100 RRab stars kpc^{-2}.

All of the panels in Figure 2 show the Bridge area. As in Paper II, we do see some RRab stars located between the Magellanic Clouds. These objects may belong to broad halos, though some evidence was found that the LMC may also have an extended disk (Saha et al. 2010; Balbinot et al. 2015;

Besla et al. 2016; Mackey et al. 2016; Nidever et al. 2019). However, again, we do not see any evident bridge-like connection between the Magellanic Clouds formed by RRL stars in any dimension—neither xz nor xy projection. Note that the xy projection is very similar to the on-sky view. The contours do connect but on a very low level (1 star kpc^{-2} and below). It is too low to state, based on the maps only, that there is an overdensity or evident connection in the Bridge area. Based on three-dimensional maps, we can only state that we do see two extended structures overlapping.

4.2. Numerical Analysis

To analyze our RRab sample quantitatively, we performed a multi-Gaussian fitting to our cleaned sample. We approximate the spatial distribution using a Gaussian mixture model with 32 components. The underlying space density of stars is approximated as a sum of Gaussians. Their relative weights and parameters (means, covariances) are found using an expectation-maximization algorithm (Dempster et al. 1977) implemented in the Python scikit-learn package (Pedregosa et al. 2011). We tested whether the multi-Gaussian fitting properly describes our data by comparing histograms of the real distribution of stars with the simulated ones. We did not specify any parameters—only the number of Gaussians and the three-dimensional locations of stars from our sample. We separately tested models with 32, 64, 128, and 256 Gaussians and did not find any significant difference between the obtained results.

Results of the multi-Gaussian procedure for 32 Gaussians are shown in Figure 3, where we overplotted Gaussian centers on the three-dimensional distribution of RRab stars from our sample. Each resulting Gaussian is represented with an open circle. The circle size marks the number of stars included in
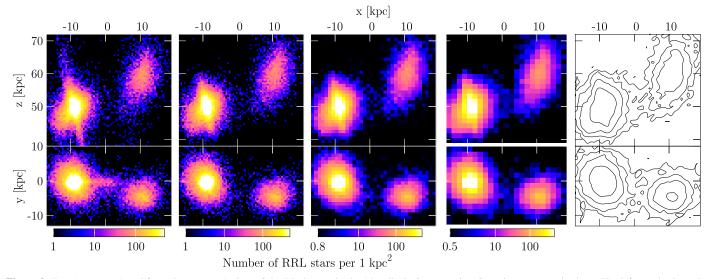
Figure 2. Top (upper row) and front (bottom row) view of the RRab stars in the Magellanic System using Cartesian space projections. The left panels show the uncleaned sample. The blend artifact, a nonphysical structure seemingly emanating from the LMC center, is very clearly visible. Note the characteristic shape the blend artifact represents in the Cartesian xy projection, which is not identical to the on-sky view (and the observer is located at $(0, 0, 0)$. The blend artifact is not protruding and elongated in the other panels, where we show the cleaned sample. The three middle panels present the same sample but with different bin sizes of (left to right) 0.5, 1, and 1.5 kpc. The right panels show the contours fitted to the middle panels (medium-sized bins, 1 kpc). Contours are on the levels of 1, 5, 20, and 100 RRab stars kpc^{-2}. The lines do connect but on a very low level.
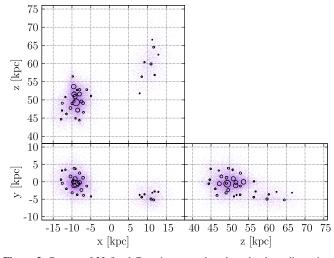

Figure 3. Centers of 32 fitted Gaussians overplotted on the three-dimensional distribution of RRab stars from the cleaned sample to which the fit was performed. Each Gaussian center is represented as an open circle, while the circle size marks the number of stars included in each Gaussian. No Gaussian is centered in the genuine Bridge area, leading to the conclusion that there is no additional population or overdensity located there.

Figure 4. Two-dimensional plots of three-dimensional Cartesian space projections showing points simulated using a multi-Gaussian fit. The top panel shows binned data, while the bottom panel shows fitted contours (black lines) and Gaussian centers (red points). Each column represents a different separation between the LMC and SMC samples, starting with 8 kpc in the left column and decreasing by 2 kpc toward the right. The right column shows points simulated for no additional offset. The bin size is 1 kpc along every axis, and the color scale is the same in each plot in the top panel. The contours are on the same levels as in Figure 2, namely 1, 5, 20, and 100 RRab stars kpc^{-2}.

each Gaussian: the smallest circle represents 237 objects, and the largest represents 2362 objects. The circle radius increases linearly with the number of objects.

Figure 3 shows that all of the Gaussians are centered in either the LMC or SMC, and none of them is centered in the genuine Bridge area. This leads to the conclusion that there is no additional population or overdensity located there. Note that this does not mean that there are no stars in the Bridge, as the Gaussians have their own individual spread. The Bridge RRab stars are thus modeled as objects located in the Gaussian wings.

To show how and when the contours connect, we use a multi-Gaussian fit to simulate the distribution of objects in the Magellanic System while adding an offset to each Magellanic Cloud sample. We use the three-dimensional Cartesian coordinates of our cleaned sample and add an offset to the x
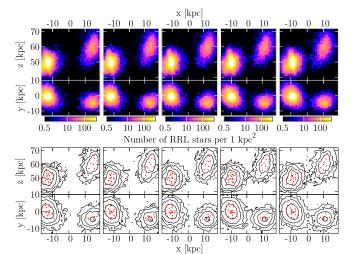
coordinate of each Magellanic Cloud sample separately for the LMC and SMC. We then fit the Gaussians and simulate the locations of the exact number of points that are included in our cleaned sample, precisely 27,212. We bin the data and fit contours. The results are shown in Figure 4. The top panel shows binned data with color-coded column density, while the bottom panel shows contours (black lines) and Gaussian centers (red points). The bin size and contour levels are the same as in the middle and right columns of Figure 2. The total offset added or subtracted from the x coordinate decreases from left to right. In the left column, the offset is 8 kpc (4 kpc added in the case of SMC, 4 kpc subtracted for the LMC), and it

decreases by 2 kpc in each column. The right column shows the simulated data with no additional offset. Comparing this column to the middle column of Figure 2, it is clearly visible that the multi-Gaussian fit reconstructs the real three-dimensional distribution of our data very well.

In the left column, where the distance between the LMC and SMC is largest, the contours do not connect, and these galaxies are separated. Once we reduce the offset, the lowest contours finally connect at a level of 2 kpc of additional offset. The galaxies' outermost regions seem to merge as the Clouds are at their current natural separation. This occurs in both the *xy* and *xz* Cartesian planes shown in Figure 4. This simulation shows that the effect of merging contours is natural for galaxies that are close enough. It does not necessarily imply that there is an additional structure between these objects, i.e., the Bridge, as the model itself has proven that there is no overdensity located in the genuine Bridge area.

However, one can argue that the lowest contours are spread more in the direction toward the MBR than in any other direction (in every plot in Figure 4). In order to verify this, we would need to significantly improve our analysis, and this is beyond the scope of this paper. First, we would need to abandon the σ-clipping and choose another method of rejecting outliers that would take into account the real error distribution, which is not normal in the case of PL relations (Nikolaev et al. 2004; Deb et al. 2018). By using σ-clipping, we probably remove some of the objects that are truly located at lower and higher distances in the outskirts of the LMC and SMC. Thus, the lowest contours perpendicular to the line of sight should not be used in such a detailed analysis. Second, we would need to observe the entire LMC outskirts located in the eastern, northern, and southern directions. Even though OGLE has lately significantly improved its sky coverage in the Magellanic System, it is still not sufficient for such an analysis, where we need to compare the very lowest contours.

Summarizing this subsection, we want to emphasize that comparison of the lowest-level contours is not sufficient to state whether or not there exists a bridge-like connection between the Magellanic Clouds.

5. A Reanalysis

The results that we presented in the previous section agree with our findings from Paper II. We do not see any evident connection in the MBR area but rather only two extended structures in the LMC and SMC outskirts that are overlapping. Recently, B17 also presented a map of the OGLE RRL stars in the Magellanic System (their Figure 18). This map clearly shows a connection between the Magellanic Clouds that was supposed to be consistent with the *Gaia* DR1 RRL candidate distribution presented in their paper. This seems to be in contradiction with any of our results—for comparison, see Figure 16 from Paper II or Figure 2 in this paper. We tried to reconstruct the results from B17. In this subsection, we describe the method that we used to reanalyze the OGLE sample of RRab stars.

5.1. No Evident Connection

In order to thoroughly check whether we actually see the connection in the OGLE data, we have reanalyzed the entire sample of RRab stars. To reproduce the B17 map precisely (their Figure 18), we have once again calculated metallicities and distance moduli using the same technique as they did

(V. Belokurov 2019, private communication). In the next paragraphs, we describe this method, and later, we discuss our results.

We used the Smolec (2005) relation for the OGLE *I* band to calculate the metallicity of each RRL star. This relation was derived for Fourier sine decomposition, and Soszyński et al. (2016) gave coefficients for the cosine decomposition; thus, we transformed the ϕ_{31} coefficient before applying the Smolec (2005) relations:

$$\phi_{31,\sin} = \phi_{31,\cos} + \pi. \tag{1}$$

The relation is (Equation (2) from Smolec 2005)

$$[\text{Fe/H}] = -3.142 - 4.902P + 0.824\phi_{31}. \tag{2}$$

Then we transformed [Fe/H] to *Z* using Equations (9) and (10) from Catelan et al. (2004),

$$\log Z = [\text{Fe/H}] + \log(0.638f + 0.362) - 1.765, \tag{3}$$

where $f = 10^{[\alpha/\text{Fe}]}$. We assumed $[\alpha/\text{Fe}] = 0$ following B17, although Carney (1996) suggested $[\alpha/\text{Fe}] = 0.30$ based on stellar clusters. We have tested both options in our analysis and found that this value does not influence our main conclusions. Then we used theoretical calibrations of the PL relations from Catelan et al. (2004) to calculate the absolute magnitudes of the RRab stars. Their Equation (8) shows a quadratic dependency between metallicity and absolute *V*-band magnitude,

$$M_V = 2.288 + 0.8824 \log Z + 0.1079 (\log Z)^2, \tag{4}$$

and Equation (3) from Catelan et al. (2004) for the *I*-band absolute magnitude,

$$M_I = 0.4711 - 1.1318 \log P + 0.2053 \log Z, \tag{5}$$

where *P* is the fundamental mode pulsation period.

Having absolute magnitudes, we were able to calculate color excesses,

$$E(V - I) = m_V - m_I - (M_V - M_I), \tag{6}$$

where $m_{V,I}$ are the observed mean magnitudes. We used the value obtained by Nataf et al. (2013), $dA_I/d(E(V-I)) = 1.215$, and assumed that $A_I = 1.215 E(V - I)$. Note that these values were obtained for the Galactic bulge, where the extinction is nonuniform and anomalous (standard extinction is around 1.5; see Udalski 2003). However, we decided to apply values from Nataf et al. (2013) in order to exactly follow the procedure used by B17.

In the last step, we calculated distance moduli using magnitudes in the *I* passband:

$$\mu_0 = m_I - M_I - A_I. \tag{7}$$

The reproduced map is shown in the bottom panel of Figure 5, and the original map from B17 is shown in the top panel. Both plots show the OGLE RRab sample, though in the case of our map (bottom panel), we used the updated sample. Both plots present samples with the same cuts: distance moduli falling into the range $18.5 < m_I - M_I < 19$ and metallicities [Fe/H] < −1.5, as well as other parameters including coordinates, sphere projections, method of calculation, bin sizes and ranges, and color-scale range. Under all of these conditions, we were able to reproduce the connection visible in the B17 map. The bridge-like structure is visible only on a very low level of counts. Moreover, due to the large bin size and
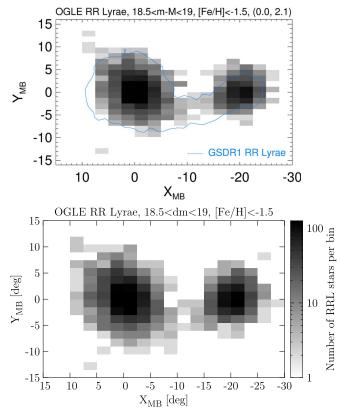
OGLE RR Lyrae, 18.5<m-M<19, [Fe/H]<-1.5, (0.0, 2.1)

OGLE RR Lyrae, 18.5<dm<19, [Fe/H]<-1.5

Figure 5. Top: bottom panel of Figure 18 from B17 showing OGLE RRab stars in the Magellanic System. The data are binned into rectangles, and a gray color scale is applied to show the column density. We only show RRab stars with distance moduli falling into the range $18.5 < m_I − M_I < 19$ and metallicities [Fe/H] $< −1.5$. The scale is logarithmic and limited to 10^0–$10^{2.1}$ RRab stars deg^{-2}. The blue contour represents the density of *Gaia* DR1 RRL candidates analyzed by B17. The coordinates used are in the MBR system, and the sky projection is not equal-plane. Bottom: our map showing OGLE RRab stars in the Magellanic System with parameters calculated using the same method as in B17. Note that the bridge-like structure is even more visible due to the elongation of bins along the connection (and equator).

elongation of bins along the *x*-axis, and thus along the Bridge, the connection is even more pronounced.

To test whether the choice of coordinate system also influences the visibility of the bridge-like connection, we plotted the same sample as in Figure 5 using different transformations. The top panels of Figure 6 show the same rectangular bins with a gray color scale but using an equal-area Hammer projection applied to the MBR (top row) and equatorial (bottom row) coordinate systems.

In the left column of Figure 6, where the color-scale range starts at 1 star deg^{-2}, the connection is not visible in either coordinate system. It only starts to emerge in the second column, where the bottom of the color-scale range is under the level of 1 star deg^{-2}—namely, 0.3. The bridge-like structure is even more pronounced in the third column, where the range is even lower. However, in the latter plot, other extended features are starting to emerge. Moreover, comparing the top and bottom gray rows demonstrates that the connection is more clearly visible in the MBR coordinates. This is due to the fact that in this system, the bridge-like structure is located along the equator. Comparing contours for both coordinate systems, we conclude that the contours do connect in both cases but on a

very low level. Again, the connection is slightly more visible in the MBR coordinate system.

Furthermore, to test whether the binning influences the results, we also plotted the same sample using square bins of different sizes. Results are shown in the bottom panels of Figure 6. Similarly to the gray panels, the top row shows the MBR, and the bottom row shows the equatorial coordinates. Comparison of rectangular and square bins leads to the conclusion that binning does indeed have an impact on the visibility of the bridge-like structure. The square bins make the connection appear significantly less visible than the rectangular bins. This is not a surprise, as the rectangular bins used by B17 were aligned with the bridge.

6. B17 RRL Candidates from *Gaia* DR1

6.1. Selection Process

In this section, we present the results of an analysis of the *Gaia* DR1 data (Gaia Collaboration et al. 2016) performed the same way as in B17. The main goal of B17 was to select RRL candidates from *Gaia* DR1 and analyze the on-sky distribution of these stars in the Magellanic System area, with an emphasis on the Bridge. They found that there is an evident connection between the Magellanic Clouds. Hereafter, we try to reproduce their results and compare with the OGLE and *Gaia* DR2 databases.

In order to reproduce the B17 list of RRL candidates using *Gaia* DR1, we use their procedure with the following steps.

1. From the entire *Gaia* DR1 database, we selected all sources located in an area where R.A.$\in(0^h, 9^h) \cup (22^h, 24^h)$ and decl. $\in(−85°, −45°)$ with more than 70 CCD crossings and Galactic longitude $b \leqslant −15°$. The latter two requirements are corresponding to *iv* and *vii* cuts from B17 (see their Section 3.3).

2. An appropriate value of extinction $E(B − V)$ was found for all sources using Schlegel et al. (1998) maps. This allowed us to deredden all of the objects from the selected sample using the following relation for the extinction coefficient for the *Gaia* G band (Equation (1) from B17), A_G:

$$A_G = 2.55E(B − V). \tag{8}$$

3. Then we calculated the amplitude value, Amp, using the following relation (Equation (2) from B17):

$$\mathrm{Amp} = \log_{10}\left(\sqrt{N_{\mathrm{obs}}}\frac{\sigma_{\overline{I_G}}}{\overline{I_G}}\right), \tag{9}$$

where N_{obs} is the number of CCD crossings, $\overline{I_G}$ is the mean flux in the *Gaia* G band, and $\sigma_{\overline{I_G}}$ is the error of the mean flux.

4. Finally, the remaining cuts presented in Section 3.3 of B17 were applied. The cuts concern amplitude as defined above, astrometric excess noise (AEN), *G*-band magnitude, and reddening.

We applied different versions of cuts *ii* and *vi* as presented in B17. We use both strict and weak cuts on the amplitude, $−0.75 < \mathrm{Amp} < −0.3$ and $−0.65 < \mathrm{Amp} < −0.3$, respectively. Similarly for the AEN, $\log_{10}(\mathrm{AEN}) < −0.2$ is a strict cut, and $\log_{10}(\mathrm{AEN}) < −0.2$ is weak. Additionally, we analyzed an even weaker version of the AEN cut, where $\log_{10}(\mathrm{AEN}) < 0.3$. Results are presented in Figure 7.

Magellanic Bridge coordinates

Equatorial coordinates

Number of RRL stars per 1 square degree

Magellanic Bridge coordinates

Equatorial coordinates

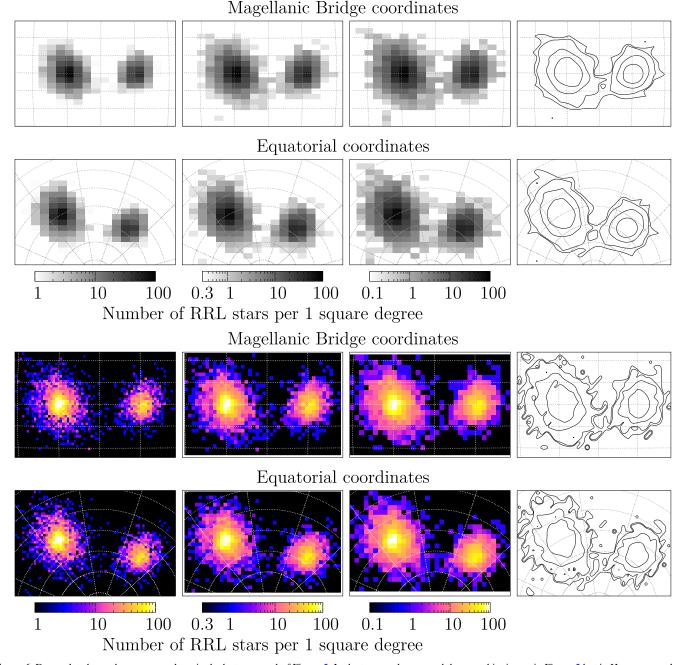Number of RRL stars per 1 square degree

Figure 6. Every plot shows the same sample as in the bottom panel of Figure 5. In the top panels, we used the same binning as in Figure 5 but in Hammer equal-area projection applied to the MBR (top row) and equatorial (bottom row) coordinate system. Each column shows a different bottom range of color scale. The right column shows contours that are on the levels of 0.5, 1, 5, and 15 RRab stars deg^{-2}. In the bottom panels, we used square bins instead of rectangular ones. We also applied a different color scale with a different range to show the subtlest features. The bin size is linearly different between each column. The top row shows the MBR, while the bottom row shows the equatorial coordinate system. Both are represented using Hammer equal-area projection. Additionally, the right column shows contours fitted to the binning shown in the second column. The contours levels are 0.5, 1, 5, and 15 RRab stars deg^{-2}.

6.2. Two-dimensional Analysis

Figure 7 clearly shows that when using the Amp and AEN cuts, both in strict versions, there are not many stars left in between the Magellanic Clouds. To test whether this result reproduces the RRL bridge reported by B17, we binned the data in the same way as their Figure 11. The bins are on too low a level, and no connection is visible; thus, strict cuts do not reproduce their bridge. Moreover, the sample we obtained using strict versions of cuts consisted of ∼7000 objects, which is three times less numerous than the B17 sample (∼21,500 objects). In the case of applying at least one cut in the weak

version, we obtained a distribution revealing stripes in the Bridge area.

The right panel of Figure 5 in B17 shows an on-sky distribution of all nominally variable stars selected from DR1. Many nonphysical features are visible, including the artifact east of the LMC. A detailed analysis of the stripes appearing in this plot was performed by B17 (for details, see their Section 3.2 and Figure 6). These stripes are aligned with the *Gaia* scanning pattern and caused by cross-match failures. Thus, most of the sources forming the stripes are not physical. Further, B17 claimed that the stripes disappear due to the cuts
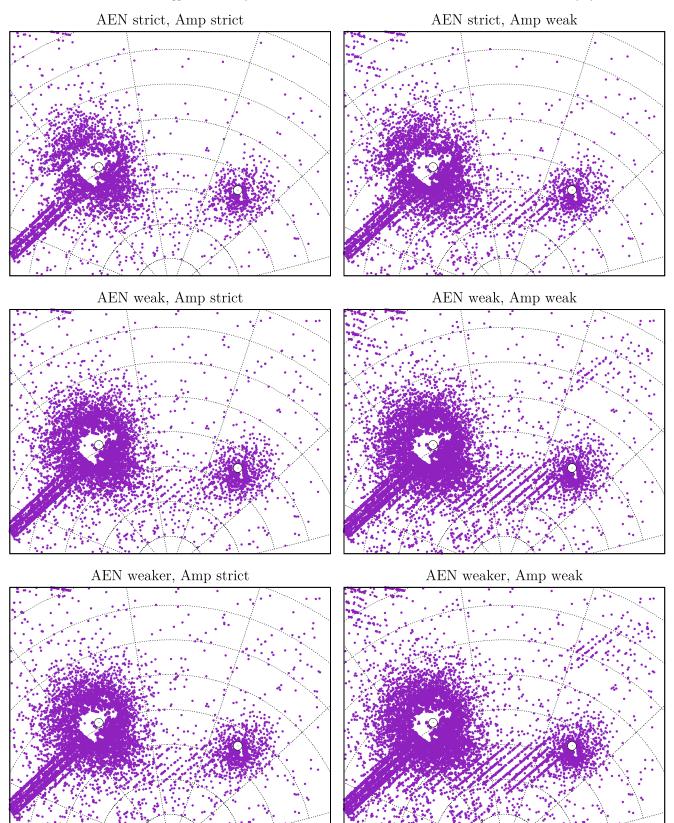
Figure 7. On-sky locations of RRL candidates using different versions of B17 cuts. Clearly visible is the nonphysical artifact east of the LMC that we did not remove. It is created by spurious variables, which are caused by *Gaia* DR1 cross-match failures (B17). Stripes are the matching *Gaia* scanning pattern. Similar stripes visible in the Bridge area suggest that many of the objects located there are nonphysical sources. Additionally, white circles mark the LMC (van der Marel & Kallivayalil 2014) and SMC (Stanimirović et al. 2004) centers.

Figure 8. Comparison of the top panel of Figure 11 from B17 (top panel) with the map obtained using the same technique (bottom panel). The bottom panel shows a sample with strict Amp cut and weaker AEN cut.

applied, and only a small number of spurious sources fall into the selected RRL regions. Our study reveals that this is not the case and that the final RRL candidate sample still contains a number of nonphysical sources forming the stripes. Comparing our Figure 7 with Figure 5 from B17, it is clearly visible that the features in the MBR area are not removed by the applied procedure. Thus, the discovery of the bridge-like connection by B17 was likely based on a nonphysical structure.

Moreover, clearly visible in Figure 7 is a nonphysical artifact located east of the LMC that we did not remove. This feature is located in the area most influenced by cross-match failures in *Gaia* DR1 (see masked pixels in the left panel of Figure 5 in B17). The sources in between the Magellanic Clouds are forming stripes that are aligned with the nonphysical artifact east of the LMC. This supports our conclusion from the previous paragraph that the Bridge area is highly influenced by nonphysical sources. Additionally, we obtain a distribution close to the center of the LMC, where the sources are missing, due to the requirement of $N_{\mathrm{obs}} > 70$. However, we managed to recreate the sample in the MBR, which is our main area of interest.

As our final sample of RRL candidates, we selected the one with a strict cut on Amp and weaker cut on AEN, as it perfectly reproduced a sample of 113 central Bridge objects from the B17 analysis (V. Belokurov 2019, private communication). In Figure 8, we show a comparison of a binned map of this sample with Figure 11 from B17. Both maps are plotted using the same coordinate system, sphere projection, bin size, and color-scale range. We managed to reproduce the Bridge features

Table 2
B17 RRL Candidates from *Gaia* DR1: Cross-match

Sample	No. Obj.	Cross-match with			
		OGLE RRL		*Gaia* DR2 RRL	
Entire	13,327	5516	(41.4%)	4872	(36.6%)
MBR	6041	2971	(47.5%)	2542	(42.1%)
Cen. MBR	113	17	(15.0%)	15	(13.3%)

Note. The MBR sample consists of objects located in the range $-20° < X_{MB} < 0°$. The central MBR sample consists of objects located between the Magellanic Clouds that contribute to B17 overdensity.

very well. One main difference between our map and that of B17 is the nonphysical artifact located east of the LMC. Note that in this binning, the *Gaia* stripes are not visible. The sample we select as our final one contains more than 13,300 stars. This is more than half of the B17 sample, indicating that they have applied even weaker cuts in their final sample.

In Figure 9, we also show our final sample using square bins of different sizes. We represented the data in the MBR coordinates using Hammer equal-area projection. As the bin size increases from left to right, the *Gaia* stripes appear less visible. The contours shown in the right panel match very well contours obtained by B17 (see their Figure 12).

6.3. Comparison with OGLE and Gaia DR2

The OGLE collection of RRL stars in the Magellanic Clouds is nearly complete—the level of completeness is higher than 95% (Soszyński et al. 2016, 2017). Therefore, we cross-matched the list of RRL candidates obtained in this section with the OCVS to test how many of these objects are genuine RRL stars. We separately cross-matched the entire sample of B17 DR1 RRL candidates and a subsample created by selecting only objects in the Bridge area located between the LMC and SMC centers. This Bridge subsample consists of sources located within $-20° < X_{MB} < 0°$.

Results are presented in Table 2, which shows that only about 41.4% of the objects in the entire RRL candidate sample are genuine RRL stars. For the Bridge subsample, this ratio is at the level of about 47.5%. Moreover, we separately tested a subsample of 113 objects in the central Bridge area, where the B17 overdensity is located. Only 17 of these objects are RRL stars, which leads to a total ratio of 15.0%. The difference between this ratio for the entire sample and the central Bridge subsample indicates a higher contamination in the latter. This is consistent with the fact that many sources in the Bridge area are nonphysical. The contamination of 85% in the central Bridge sample is not consistent with B17, who gave a value of 30%–40% for their entire sample.

Note that the area that we use for the RRL candidate selection process is larger than the OGLE-IV field coverage (see Figure 1), so our *Gaia* search window is larger than the plotted area. For the entire sample, the difference in purity level is larger than for the Bridge sample, as the former includes the nonphysical artifact in DR1 data that is not entirely covered by the OGLE fields. For the Bridge sample, only a few sources are located north and south of the OGLE footprint. Thus, this effect should not be significant for the selected Bridge subsample. It also explains the significant difference between the cross-matches of RRL candidate samples with the OGLE data.

We would expect that a proper technique of selecting RRL candidates would lead to a result of high completeness. To test
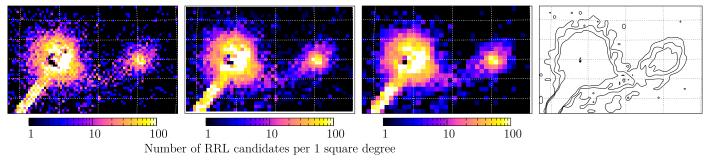
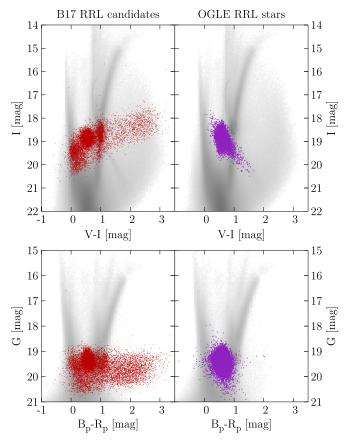**Figure 9.** Same sample as in Figure 8 (bottom panel) but binned using square bins.

Figure 10. The CMDs of the B17 RRL candidates (left; red) obtained in this section and the cleaned sample of OCVS RRL stars (right; purple) overplotted on the Hess diagrams for the data from selected fields in the Magellanic System. Top: OGLE photometry. Bottom: *Gaia* DR2 photometry.

that, we compared the number of RRL stars from our reconstructed sample using the described technique to the total number of these objects in the OGLE database in the Magellanic System. The entire RRL candidate list has a completeness level of 11.6%, while for the Bridge sample, it is 12.4%, which is consistent with what B17 estimated. This means that almost 90% of RRL stars located in the OGLE-IV fields in the Magellanic System were not discovered in the reconstructed sample of B17.

Moreover, we also cross-matched the obtained RRL candidate lists with the entire OCVS published to date and the entire OGLE database. About 2.3% of objects from the candidate samples are eclipsing binaries. A few are also classified in the OCVS as long-period variables. We show in Figure 10 a comparison of the color–magnitude diagram

(CMD) of the sample obtained in this section with the cleaned sample of RRL stars. Both are overplotted on the OGLE (top panels) and *Gaia* DR2 (bottom panels) data from selected fields in the Magellanic System. The reconstructed B17 sample spans different areas than those usually occupied by the genuine RRL stars. Thus, this sample contains a lot of different types of objects.

We have also performed a cross-match between the RRL candidate sample from *Gaia* DR1 obtained in this section and the *Gaia* DR2 RRL stars listed in the vari_rrlyrae table (Gaia Collaboration et al. 2018; Holl et al. 2018; Clementini et al. 2019). Table 2 lists the exact results. Only about 37% of sources from the RRL candidate sample are present in the *Gaia* DR2. For the Bridge sample, this result is slightly higher: 42%. Lower numbers as compared to the cross-match with the OGLE data are probably a result of lower DR2 RRL sample completeness, which we describe in the following section.

7. Comparison of Different Tracer Distribution

In this section, we compare on-sky distributions of different tracers in the MBR area. The main plot that we discuss is shown in Figure 11. The first row contains the H I density contours from the Leiden/Argentine/Bonn H I Survey (Kalberla et al. 2005; same as Figure 8 in Skowron et al. 2014) and the Galactic All Sky H I Survey (McClure-Griffiths et al. 2009; Kalberla et al. 2010; Kalberla & Haud 2015) and the young population, red clump, and top and bottom of the red giant branch (RGB) distributions (Figures 8, 9, 11, and 13 from Skowron et al. 2014). The middle row shows the different types of classical pulsators from the OCVS that we investigated in Paper III and this paper, namely classical Cepheids (CCs), anomalous Cepheids (ACs), both these types plotted together, RRabs of the cleaned sample, RRabs of the entire sample, and RRLs of all types plotted together. Similarly, these types of objects are shown in the bottom row using data from *Gaia* DR2 (with the exception of the cleaned RRab sample that we calculated only for the OCVS). All of these plots show a color-coded column density, while lines represent density contours. For each plot, the color scale and contour levels are different.

Comparing neutral hydrogen with other maps, it is clearly visible that the most matches are distributions of young stars and CCs. Each of these three seems to follow a bridge-like connection between the Magellanic Clouds along a similar decl. range: decl.$\in$(70°, 72°). Older tracers are more spread out and do not follow such strict connection. Red clump and RGB bottom stars are more concentrated in the southern parts of the Bridge than RGB top and RRL stars. The RGB top objects are very spread out, and the lowest-density contours show some clumps, with the most populated stripe located along the young
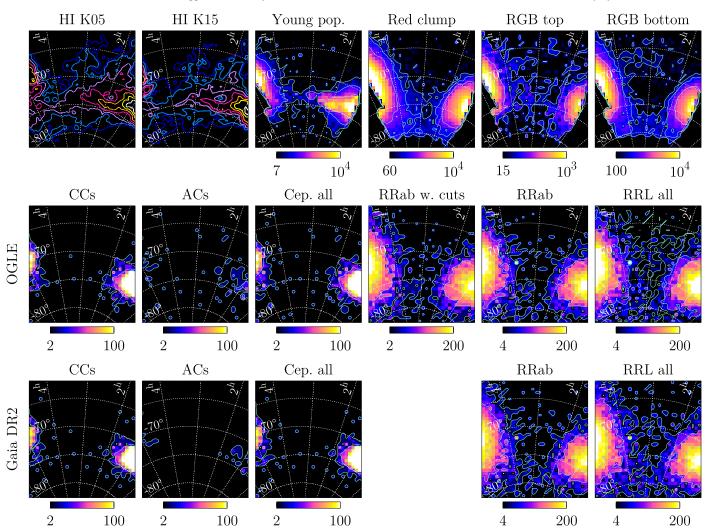
Figure 11. Comparison of on-sky locations of different tracers in a Hammer equal-area projection. Each plot has its own color scale and contour levels. Top row: The first panel shows neutral hydrogen density contours from the Leiden/Argentine/Bonn H I Survey (Kalberla et al. 2005, the same as in Figure 8 in Skowron et al. (2014); see that figure description for details). The second panel shows H I from the Galactic All Sky H I Survey (McClure-Griffiths et al. 2009; Kalberla et al. 2010; Kalberla & Haud 2015). Contours are on the levels (1, 2, 4, 8, 16, 32, 64) · 10^{20} cm^{-2}. In both panels, the H I is integrated over the velocity range 80 km s^{-1} < v < 400 km s^{-1}. The third to fifth panels show column densities of different stellar populations as selected in the CMDs in Skowron et al. (2014). Shown here for comparison are the young population, red clump objects, and the top and bottom of the RGB. Middle row: classical pulsators from the OCVS. Bottom row: classical pulsators from the *Gaia* DR2.

population bridge. However, the connection is on too low a level to enable us to state that we see a connection similar to the young bridge. Summing up, for all intermediate-age and older tracers from Skowron et al. (2014), we can see two extended structures overlapping with no evident bridge-like connection.

The RRL star on-sky distribution shows that these stars are very spread out in many directions—even more than the other tracers that we discussed in the previous paragraph. Among the presented distributions, the distribution of RGB stars is the most similar to the distribution of RRL stars. The difference between the RRab cleaned and entire samples shows that a number of objects are rejected from the Bridge sample. Note, however, that the column density in this area is low, and removing even a small number of objects can result in a significantly different density contour distribution. The entire RRab sample is distributed very similarly to all RRL types, though the lowest-density contours are slightly different. This is caused by the fact that the entire RRL sample is more numerous. Moreover, one can state that the ACs are similarly spread out as the intermediate-age and older tracers. On the

other hand, the ACs sample is significantly less numerous. We do not discuss further differences or similarities between different types of classical pulsators in this paper; for a detailed statistical study of three-dimensional distributions, see Iwanek et al. (2018).

Figure 11 shows that in DR2, many ACs were classified as CCs. This is the main reason for the differences between the OCVS and DR2 CC distributions. For a detailed description, see Section 7 in Paper III. Note also that Ripepi et al. (2019) recently reclassified the DR2 sample of CCs. For a comparison, see Figure 12 in Paper III. The *Gaia* DR2 RRL stars are distributed very similarly to the OGLE RRL stars, both RRab and all types of these pulsators. These objects are very spread out, and while the lowest-density contours do connect, it occurs on a very low level, below 1 star deg^{-2}. Thus, this cannot be the reason for stating that we see an evident bridge-like connection; we actually do not.

Using our updated OGLE sample of RRL stars and the *Gaia* DR2 sample, we performed a cross-match between these two. Similarly to Paper III, we selected a DR2 sample covering the

entire OGLE field in the Magellanic System. In this area, *Gaia* DR2 has a completeness of 69.0% for all RRL stars. This value is consistent with Table 2 in Holl et al. (2018). Again, this is not surprising, as the OGLE collection of RRL stars was a training set for the *Gaia* selection algorithms.

8. Conclusions

In this paper, closely following our analysis of CCs in the MBR area (Paper III), we present a detailed study of RRL stars in between the Magellanic Clouds using an extended OCVS (Soszyński et al. 2016, 2017, 2019). We calculated absolute Wesenheit magnitudes for each RRL star, starting with estimating photometric metallicities (Nemec et al. 2013) and applying Braga et al. (2015) relations. This led to us calculating individual distances for our sample, the same technique as in Paper II and Skowron et al. (2016).

We analyzed a three-dimensional distribution of RRL stars between the Magellanic Clouds in Cartesian coordinates. We show—confirming the results from Paper II, as well as Wagner-Kaiser & Sarajedini (2017)—that we do not see an evident connection between the Magellanic Clouds in RRL stars. Objects located in the Bridge area form a smooth transition between the Clouds, rather than a bridge-like connection. The RRL distribution seems to represent two extended structures overlapping (i.e., halos or extended disks of the LMC and SMC). Additionally, we bin the data and show that the contours do connect, though on a very low level (below 1 star deg^{-2} or kpc^{-2}). It is too low to state that an evident overdensity exists.

To test our sample numerically, we performed a multi-Gaussian fit. We made only two assumptions: the number of Gaussians and the number of points to be simulated. Our results show that there is no Gaussian centered in the Bridge area. Thus, there is no additional population or overdensity therein. We also used the multi-Gaussian procedure to show that when we separate the Magellanic Clouds by 8 kpc along the Cartesian x-axis, and then gradually shift the LMC and SMC back together, the lowest-density contours start to connect at some point. Thus, the fact that the contours connect is not necessarily evidence of the existence of an old bridge, as any contours will connect when the galaxies are close enough.

Moreover, to carefully study the lowest-density contours, one needs to use a very precise technique to classify and analyze RRL stars. Even though the method we use is quite robust, as it is used in many different studies of three-dimensional structure, we do not think that it is precise enough to test the very outskirts of the Magellanic Clouds.

Lately, B17 presented a distribution of OGLE RRL stars in the Bridge that revealed a bridge-like connection (see their Figure 18). This is in contradiction with results from Paper II or even from this paper that were described earlier. We reanalyzed our OGLE sample using a different technique to test consistency. We show that the way the data are plotted influences the final impression. Carefully testing how the sample looks in different coordinate systems and using different bin sizes and types of bins, we show that we are able to reproduce the B17 plot only under specific conditions. Thus, because the connection is not always visible, we are even more convinced that it is on a very low level.

Using the same method as B17, we also reproduced their main results by selecting RRL candidates from *Gaia* DR1 data. We applied a series of cuts to the data, as presented in B17.

When all of the selection methods are used in strict versions, we obtain a very small number of objects in between the Magellanic Clouds. On the other hand, if at least one cut is weaker, the resulting distribution contains many spurious sources in the MBR area. Thus, we conclude that we are not able to reproduce the B17 RRL bridge without nonphysical artifacts, and we do not agree with their statement that the cuts presented remove most of the spurious sources. We also present a map of selected objects showing very evident stripes that, according to B17, match the *Gaia* overlapping fields. This nonphysical overdensity is matching the B17 discovery very well. In the central Bridge area, only 15% of the sample are genuine RRL stars.

We also show, for the first time, the distribution of *Gaia* DR2 RRL stars in the MBR and compare it to the OCVS. On-sky locations of RRL stars from both samples are very consistent. Similarly to the OCVS RRL stars, the DR2 sample reveals a very spread out distribution that more resembles two overlapping structures than a strict bridge-like connection. The lowest-density contours do connect, though on a very low level, again below 1 star deg^{-2}. These contours look slightly different when using only RRab stars instead of the entire RRL sample. This is probably due to the latter being more numerous. Again, we conclude that the existence of a bridge-like structure should not be based on the lowest-density contours.

At the same time, we want to emphasize that we do not state that the RRL bridge does not exist. There are different surveys showing that there are some substructures in between the Magellanic Clouds. This is in agreement with our own study, as we also show that there are RRL stars in the Bridge area, though their distribution is not very bridge-like, and the overdensity is on a very low level.

ORCID iDs

Anna M. Jacyszyn-Dobrzeniecka ● https://orcid.org/0000-0002-5649-536X
Przemek Mróz ● https://orcid.org/0000-0001-7016-1692
Igor Soszyński ● https://orcid.org/0000-0002-7777-0842
Patryk Iwanek ● https://orcid.org/0000-0002-6212-7221
Jan Skowron ● https://orcid.org/0000-0002-2335-1730
Paweł Pietrukowicz ● https://orcid.org/0000-0002-2339-5899
Radosław Poleski ● https://orcid.org/0000-0002-9245-6368
Szymon Kozłowski ● https://orcid.org/0000-0003-4084-880X
Krzysztof Ulaczyk ● https://orcid.org/0000-0001-6364-408X

References

Bagheri, G., Cioni, M.-R. L., & Napiwotzki, R. 2013, A&A, 551, A78
Balbinot, E., Santiago, B. X., Girardi, L., et al. 2015, MNRAS, 449, 1129
Belokurov, V. A., & Erkal, D. 2018, MNRAS, 482, L9
Belokurov, V. A., Erkal, D., Deason, A. J., et al. 2017, MNRAS, 466, 4711
Besla, G., Kallivayalil, N., Hernquist, L., et al. 2010, ApJL, 721, L97
Besla, G., Kallivayalil, N., Hernquist, L., et al. 2012, MNRAS, 421, 2109
Besla, G., Martínez-Delgado, D., van der Marel, R., et al. 2016, ApJ, 825, 20
Braga, V. F., Dall'Ora, M., Bono, G., et al. 2015, ApJ, 799, 165
Carney, B. W. 1996, PASP, 108, 900
Carrera, R., Conn, B. C., Nöel, N. E. D., et al. 2017, MNRAS, 471, 4571
Catelan, M., Pritzl, B. J., & Smith, H. A. 2004, ApJS, 154, 633
Clementini, G., Ripepi, V., Molinaro, R., et al. 2019, A&A, 622, A60
Connors, T. W., Kawata, D., & Gibson, B. K. 2006, MNRAS, 371, 108
Deason, A. J., Belokurov, V., Erkal, D., Koposov, S. E., & Mackey, D. 2017, MNRAS, 467, 2636
Deb, S., Ngeow, C.-C., Kanbur, S. M., et al. 2018, MNRAS, 478, 2526
Demers, S., & Battinelli, P. 1998, AJ, 115, 154
Dempster, A. P., Laird, N. M., & Rubin, D. B. 1977, Journal of the Royal Statistical Society, 39, 1
Diaz, J. D., & Bekki, K. 2012a, MNRAS, 413, 2015
Diaz, J. D., & Bekki, K. 2012b, ApJ, 750, 36
Gaia Collaboration, Brown, A. G. A., Vallenari, A., et al. 2016, A&A, 595, A2
Gaia Collaboration, Brown, A. G. A., Vallenari, A., et al. 2018, A&A, 616, A1
Gardiner, L. T., & Noguchi, M. 1996, MNRAS, 278, 191
Gardiner, L. T., Sawa, T., & Fujimoto, M. 1994, MNRAS, 266, 567
Guglielmo, M., Lewis, G. F., & Bland-Hawthorn, J. 2014, MNRAS, 444, 1759
Harris, J. 2007, ApJ, 658, 345
Holl, B., Audard, M., Nienartowicz, K., et al. 2018, A&A, 618, A30
Irwin, M. J., Kunkel, W. E., & Demers, S. 1985, Natur, 318, 160
Iwanek, P., Soszyński, I., Skowron, D. M., et al. 2018, AcA, 68, 213
Jacyszyn-Dobrzeniecka, A. M., Skowron, D. M., Mróz, P., et al. 2016, AcA, 66, 149
Jacyszyn-Dobrzeniecka, A. M., Skowron, D. M., Mróz, P., et al. 2017, AcA, 67, 1
Jacyszyn-Dobrzeniecka, A. M., Soszyński, I, Udalski, A., et al. 2020, ApJ, 889, 25
Kalberla, P. M. W., Burton, W. B., Hartmann, D., et al. 2005, A&A, 440, 775
Kalberla, P. M. W., & Haud, U. 2015, A&A, 578, A78
Kalberla, P. M. W., McClure-Griffiths, N. M., Pisano, D. J., et al. 2010, A&A, 512, A14
Mackey, A. D., Koposov, S. E., Da Costa, G. S., et al. 2018, ApJL, 858, L21
Mackey, A. D., Koposov, S. E., Erkal, D., et al. 2016, MNRAS, 459, 239
McClure-Griffiths, N. M., Pisano, D. J., Calabretta, M. R., et al. 2009, ApJS, 181, 398
Nataf, D. M., Gould, A., Fouqué, P., et al. 2013, ApJ, 769, 88
Nemec, J. M., Cohen, J. G., Ripepi, V., et al. 2013, ApJ, 773, 181
Nidever, D., Olsen, K., Choi, Y., et al. 2019, ApJ, 874, 118
Nikolaev, S., Drake, A. J., Keller, S. C., et al. 2004, ApJ, 601, 260
Nöel, N. E. D., Conn, B. C., Carrera, R., et al. 2013, ApJ, 768, 109
Nöel, N. E. D., Conn, B. C., Read, I. J., et al. 2015, MNRAS, 452, 4222
Oey, M. S., Dorigo Jones, J., Castro, N., et al. 2018, ApJL, 867, L8
Pedregosa, F., Varoquaux, G., Gramfort, A., et al. 2011, Journal of Machine Learning Research, 12, 2825, http://www.jmlr.org/papers/volume12/pedregosa11a/pedregosa11a.pdf
Ripepi, V., Molinaro, R., Musella, I., et al. 2019, A&A, 625, A14
Růžička, A., Theis, C., & Palouš, J. 2009, ApJ, 691, 1807
Růžička, A., Theis, C., & Palouš, J. 2010, ApJ, 725, 369
Saha, A., Olszewski, E. W., Brondel, B., et al. 2010, AJ, 140, 1719
Schlegel, D. J., Finkbeiner, D., & Davis, M. 1998, ApJ, 500, 525
Shapley, H. 1940, BHarO, 914, 8
Simon, N. R., & Lee, A. 1981, ApJ, 248, 291
Skowron, D. M., Jacyszyn, A. M., Udalski, A., et al. 2014, ApJ, 795, 108
Skowron, D. M., Soszyński, I., Udalski, A., et al. 2016, AcA, 66, 269
Smolec, R. 2005, AcA, 55, 59
Soszyński, I., Dziembowski, W. A., Udalski, A., et al. 2011, AcA, 61, 1
Soszyński, I., Udalski, A., Szymański, M. K., et al. 2014, AcA, 64, 177
Soszyński, I., Udalski, A., Szymański, M. K., et al. 2016, AcA, 66, 131
Soszyński, I., Udalski, A., Szymański, M. K., et al. 2017, AcA, 67, 103
Soszyński, I., Udalski, A., Szymański, M. K., et al. 2019, AcA, 69, 87
Stanimirović, S., Staveley-Smith, L., & Jones, P. A. 2004, ApJ, 604, 176
Udalski, A. 2003, ApJ, 590, 284
Udalski, A., Szymański, M. K., & Szymański, G. 2015, AcA, 65, 1
van der Marel, R. P., & Kallivayalil, N. 2014, ApJ, 781, 121
Wagner-Kaiser, R., & Sarajedini, A. 2017, MNRAS, 466, 4138
Yoshizawa, A. M., & Noguchi, M. 2003, MNRAS, 339, 1135
Zivick, P., Kallivayalil, N., Besla, G., et al. 2019, ApJ, 874, 78